Analyst

ROYAL SOCIETY OF CHEMISTRY

PAPER

View Article Online
View Journal | View Issue

Cite this: *Analyst*, 2021, **146**, 2321

Highly sensitive detection of DNA damage in living cells by SERS and electrochemical measurements using a flexible gold nanoelectrode†

Jing Zhou,[a] Dan Yang,[a] Guohui Liu,[a] Siying Li,[a] Wennan Feng,[a] Guocheng Yang,[a] Jin He*[b] and Yuping Shan*[a]

Received 3rd February 2021,
Accepted 9th February 2021

DOI: 10.1039/d1an00220a

rsc.li/analyst

Guanine (G) oxidation products, such as 8-hydroxy-2′-deoxyguanosine (8-OHdG) and 8-oxo-guanine (8-OXOG), have been widely studied as promising biomarkers for DNA oxidative damage. In this work, we develop a new method to detect G oxidative products released from live cells after chromium (VI) ion or hydrogen peroxide treatments by using a glass nanopipette-based flexible gold nanoelectrode (fGNE). Specific response to G oxidative products with high sensitivity can be detected from the fGNE tip through integrated electrochemical measurements and surface-enhanced Raman spectroscopy. The fGNE apex can be positioned very close to the cell membrane noninvasively because of its high flexibility and nanoscale tip size. With the assistance of the electrophoretic force, the fGNEs can effectively collect and detect the G-derived DNA damage products released from individual cells in the cell culture medium with high sensitivity.

Introduction

Reactive oxygen species (ROSs), formed during endogenous metabolic processes and exposure to environmental factors, can induce various lesions in nuclear and mitochondrial DNA.[1,2] Among more than 100 types of DNA damage, guanine (G) oxidative derivatives are the most abundant forms because G is the one most susceptible to oxidation among the four DNA bases.[3,4] Fortunately, life has developed various systems to quickly detect and repair DNA damage.[2,5] The oxidized G base is mainly repaired through base excision repair (BER) and the base oxidation products, 8-oxo-guanine (8-OXOG) or its tautomer 8-hydroxyguanine (8-OHGua), are efficiently removed from the DNA strand. Meanwhile, their nucleotide forms, 8-oxo-2′-deoxyguanosine (8-OXOdG) and its tautomer 8-hydroxy-2′-deoxyguanosine (8-OHdG), can also be generated inside the cell through different repair pathways such as nucleotide excision repair (NER) or directly from the free nucleotide pool.[6,7] Both 8-OXOG and 8-OHdG have become important biomarkers of oxidative stress and reflect the dynamic balance between cellular DNA damage and repair.[8–10] It should be noted that the tautomer structures are often not clearly differentiated in the previous literature. Between the base and nucleoside forms, more analytical methods have been developed to detect and quantify 8-OHdG outside cells, which may be related to its better cross-membrane capability.[7] 8-OHdG is usually detected at an elevated level in the urine or serum of patients with increased oxidative stress or risk of diseases, including neurodegenerative diseases, cancers, cardiovascular diseases and diabetes.[11–13]

Classical analytical methods have been developed for 8-OHdG and 8-OXOG detection mainly in urine and blood samples, including high-performance liquid chromatography (HPLC),[10,14,15] gas chromatography (GC)–mass spectrometry (MS), liquid chromatography (LC)–MS,[14,16,17] and enzyme-linked immunosorbent assay (ELISA).[18,19] These methods have extremely high sensitivity (nanomolar or better) and specificity, but extensive sample preparations are needed, and only an ensemble average can be obtained. At the cellular level, 8-OXOG within the cells can often be detected by fluorescence-based methods.[8,20] However, the research is still limited to directly detect the trace amount of 8-OXOG or 8-OHdG released from individual living cells,[21] which are also critical for fundamental studies of oxidative DNA damage and early diagnosis of diseases.[22]

In recent years, various new methods have been developed for living cell sensing and analysis, especially down to the single-cell level. These new technical developments can

[a]*School of Chemistry and Life Science, Advanced Institute of Materials Science, Changchun University of Technology, Changchun 130012, China.*
E-mail: shanyp@ciac.ac.cn
[b]*Physics Department, Florida International University, Miami, 33199, USA.*
E-mail: jinhe@fiu.edu

†Electronic supplementary information (ESI) available. See DOI: 10.1039/d1an00220a

provide a new solution for the detection of G-derived DNA damage products. Because 8-OXOG/8-OHGua and their nucleotide forms can be further oxidized and thus be detected electrochemically, well-developed micro/nanoelectrode-based electrochemical (EC) techniques can be utilized.[23–25] For example, carbon fiber microelectrodes have been utilized for real-time detection of 8-OHdG released by individual lung epithelial cells after exposure to nicotine.[26] In recent years, nanoelectrode (NE) and nanopipette based electrochemical methods have made great progress for single-cell studies since they can ensure the integrity and physiological activity of the living cells during detection.[27–29] In addition to micro/nanoelectrode-based electrochemical techniques, surface-enhanced Raman spectroscopy (SERS) has been used together with nanoelectrodes and nanopipettes in qualitative single-cell analysis because of its high sensitivity and selectivity at the molecular level.[30–32] Furthermore, SERS has been successfully used to differentiate four DNA bases and has been combined with EC techniques for biosensing.[29–31] Therefore, an integrated EC and SERS approach may provide a promising new approach to probe the trace amount of oxidized G derivatives released from live cells.

In this report, we have explored an integrated EC and SERS approach for extracellular detection of oxidized G derivatives in the cell culture medium at the single-cell level. The measurements were achieved by using a glass nanopipette-based flexible gold nanoelectrode (fGNE). In the live cell experiment, the nanoscale and flexible tip of the fGNE can be positioned very close to the cell membrane with minimal damage to the cell. Without further chemical modification, the oxidized G base and nucleotide can attach to the exposed gold surface of the fGNE mainly through the strong Au–N interaction.[33,34] After treatments with the often-used DNA damage agents chromium(VI) ion[35,36] or hydrogen peroxide (H_2O_2),[20,37,38] increased amounts of oxidized G derivatives are released from individual cells and can be effectively collected by the fGNE positioned very close to the cells. The fGNE shows good responses to G oxidative products, including 8-OHdG and 8-OXOG, in differential pulse voltammetry (DPV) and SERS measurements. By comparing with spiked 8-OHdG in a controlled environment, we conclude that the fGNE-based method can detect about 0.1 nM concentration of G oxidative products in the cell culture medium.

Experimental

Reagents and materials

NaCl, KCl, $Na_2HPO_4{\cdot}2H_2O$, KH_2PO_4, trypan blue and H_2SO_4 of ACS grade or better were purchased from Shanghai Aladdin without further purification. 1×PBS was prepared from deionized water (~18.2 MΩ cm, Millipore). $AgNO_3$, $Ru(NH_3)_6Cl_3$, DNA bases (A, T, G, C), 8-hydroxy-2′-deoxyguanosine (8-OHdG), and K_2CrO_4 were purchased from Sigma-Aldrich. $HAuCl_4{\cdot}4H_2O$ and H_2O_2 were purchased from Shanghai Macklin and Beijing Chemical Works, respectively. Silver nanoparticles (AgNPs, ~59 nm) were synthesized as previously described.[39] The characterization of AgNPs is described in the ESI.†

Fabrication of the fGNE

The details of fGNE fabrication can be found in the ESI.† In brief, a clean quartz capillary (QF100-70-7.5) was pulled by using a laser pipette puller (P-2000, Sutter Instrument) with the following parameters: HEAT = 650, FIL = 4, VEL = 60, DEL = 170, and PUL = 180. The nanopore size was determined by ionic current measurements. Then CNEs were formed inside the nanopipette barrel by the pyrolysis of butane gas, which flows through the nanopipette barrel with controlled pressure.[40] The fabricated CNEs were then placed in 1×PBS solution with 10 mM $HAuCl_4$. Gold was electrochemically deposited on the CNE apex as well as the nearby glass surface at a constant −70 mV bias for 8 min (see Fig. S3†).[41] The electrode surface area was determined by the diffusion-limited current of cyclic voltammograms (CVs). The nanopipette, CNE and fGNE were also imaged by SEM (JEOL JSM-7610F).

Characterization of nanopipettes, CNEs, and fGNEs by electrochemical measurements

The electrochemical measurements of G and 8-OHdG were conducted using a potentiostat (CHI 852D). An Ag/AgCl wire electrode was used as the quasi-reference electrode (0.2 mm in diameter) and a Pt wire (0.5 mm in diameter) was used as the counter electrode. For the measurements in the controlled environment, the DPV measurements were performed in 10 mM PBS (pH 7.0–7.5) with various G or 8-OHdG concentrations. The DPV measurement of 8-OHdG was also conducted in the cell culture medium. To study G oxidation, CVs were obtained continuously with two different potential sweep rates (20 V s^{-1} and 0.05 V s^{-1}) for 50 cycles in 10 mM PBS solution with 10 μM G to obtain the oxidation products of G on the fGNE surface. Subsequently, DPV measurements were performed using fGNEs with the adsorbed oxidation products of G in 10 mM PBS solution.

SERS measurements for products of DNA oxidative damage on the fGNE

Before the SERS measurements, the fGNE tethered with products of DNA oxidative damage was placed in 10 mM PBS with about 80 pM of 59 nm size AgNPs for 5 min to enhance the SERS signal. SERS measurements were performed using a confocal Raman microscope system (Horiba LabRAM HR evolution). The samples were excited with a 532 nm laser with 20 mW power, and a ×50 objective was used in the measurements to focus the laser beam spot (about 2 μm size) on the fGNE tip. The typical exposure time was 10 s. The Raman spectral resolution was 0.3 cm^{-1}. The acquired Raman spectra were smoothened by a moving average method (neighboring 5 points) using Origin software (OriginLab).

Cell culture, DNA damage treatment, and DNA oxidative damage product collection

Three types of cells, human lung cancer cells (A549), human cervical cancer cells (HeLa), and African green monkey kidney cells (Vero), were purchased from the Institutes of Biological Sciences (Shanghai, China). A549 and HeLa cells were cultured in Dulbecco's modified Eagle's medium (DMEM), and Vero cells were cultured in minimum Eagle's medium (MEM). Each type of medium was supplemented with 10% fetal bovine serum, penicillin (100 μg mL^{-1}), and streptomycin (100 μg mL^{-1}). The cells were cultured at 37 °C in a humidified incubator containing 5% CO_2. The cells were subcultured until 80% of the Petri dish was covered by cells. For DNA damage treatment, concentrated K_2CrO_4 or H_2O_2 solution was added into the Petri dish to reach a final concentration of 20 μM, and the treatment time was always 2 h. Before measurements, cells attached to the glass slides were washed with 1×PBS and rinsed with the medium. A micromanipulator (TransferMan 4r, Eppendorf) was used to precisely control the distance between the fGNE and the cell membrane surface. The fGNEs collected the DNA oxidative damage products at an applied bias of −70 mV for different times. In the experiments of collecting DNA oxidative damage products, a temperature control system (Warner Instruments, TC-344C) maintained the temperature at 37 °C.

DFT calculation

Gaussian 09 software was used for geometric optimization and Raman spectra calculation of all four DNA bases and 8-OHdG. The Raman spectra calculations were conducted by using the functional B3LYP and the basis set 6-311+G**. A scaling factor of 0.963 was used for all the vibrational bands.

Results and discussion

Experimental setup for detecting the DNA oxidative damage products

The fabrication of fGNEs has been reported previously.[42] The details are also shown in Fig. S1.† In brief, the empty barrel of the single-barrel nanopipette was filled with a carbon nanoelectrode (CNE) after the pyrolysis of butane gas. Then, gold was electro-deposited on the exposed CNE at the orifice. Fig. 1A shows the optical microscopy images of the side view of the nanopipette (i) and fabricated fGNE tip (ii) and SEM images of the apex of the nanopipette (iii) and fGNE (iv). The mean diameter of the nanopore is about 102 ± 16 nm as determined by ionic current measurements (Fig. S2†). The cross section of the fGNE shows gold plating at the apex of the CNE. After gold deposition on the CNE, the diffusion-limited current in the CV increased by about 6-fold (see Fig. S3A†). Accordingly, the mean effective surface area increased from 0.78 ± 0.41 $μm^2$ for the CNEs to 5.06 ± 0.89 $μm^2$ for the fGNEs (Fig. S3B and C†). A stable and pronounced gold reduction peak appeared in the CV during the repeated potential scans in 0.5 M H_2SO_4 (Fig. S4†), confirming the successful fabrication of stable fGNEs.

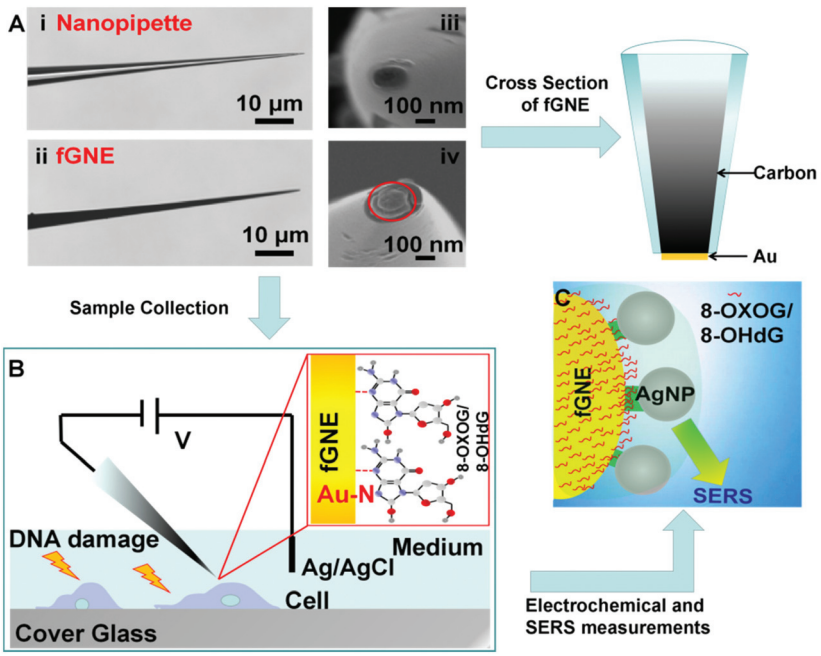

Fig. 1 Schematic diagram of the experimental setup. (A) Optical (left) and SEM images (right) of the nanopipette (i and iii) and fGNE (ii and iv). The orifice pointed by the red circle indicates the successful deposition of gold on the carbon nanoelectrode. (B) Diagram of the fGNE collecting DNA damage products (only the 8-OHdG structure is shown here) from individual cells. (C) Illustration of SERS detection of cellular DNA damage products on the fGNE with AgNPs.

In single-cell analysis, we used a micromanipulator to position the fGNE apex near the membrane surface of individual live cells that have been treated with the DNA damage agents K_2CrO_4 or H_2O_2 for 2 h (see Fig. 1B). Both reagents have often been used to induce cellular DNA damage. Fast release and increased levels of an oxidized G base and a nucleotide, including 8-OHdG and 8-OXOG, were reported.[35–38] A negative bias (−70 mV) was applied on the fGNE to help attract the negatively charged DNA damage oxidative products on to the fGNE through the relatively strong Au–N interaction.[33,43] The strong interaction between 8-OHdG and gold was also confirmed by the AuNP experiment using UV–vis spectroscopy (Fig. S5†).

The collected G and its derivatives on the fGNE apex can be detected and identified by differential pulse voltammetry (DPV) measurements based on the oxidation peak. We further used SERS to detect them. Before SERS measurements, AgNPs with a mean size of about 59 nm (Fig. S6†) were first deposited on the fGNE surface to enhance the SERS signal, as shown in Fig. 1C. Fig. S6C† shows an 8-OHdG-modified fGNE apex covered with AgNPs.

Electrochemical detection and oxidation of G and 8-OHdG

To evaluate the sensitivity and selectivity of fGNEs for detecting G and 8-OHdG, we first use the DPV method, which has a current noise level of 0.1 pA. Fig. 2A and C show the DPVs with a pronounced oxidation peak for G and 8-OHdG, respectively. The oxidation potentials are about 0.72 V for G and 0.43 V for 8-OHdG.[44,45] We also conducted the DPV measurement in the solution with both 10 μM G and 8-OHdG. Both peaks of G and 8-OHdG can be observed (Fig. S7A†). In addition, the peaks of G or 8-OHdG are also lower than the oxidation peaks of other bases and thus can be clearly differentiated in the mixture (Fig. S7B†).

The DPV peak height (ΔI_P) increases proportionally with the concentration of G or 8-OHdG in the range from 0 to 500 nM (Fig. 2B and D). The stepwise increase of ΔI_P with increasing concentrations of G and 8-OHdG shows the fast response and high sensitivity of the fGNE to G and 8-OHdG. The slopes of the ΔI_P *vs.* concentration plots for G and 8-OHdG in the range of 0–500 nM are 0.014 pA nM^{-1} and 0.018 pA nM^{-1}, respectively. With a S/N ratio of 3, the limits of detection (LoDs) for G and 8-OHdG are 5 nM and 10 nM, respectively, under the conditions of a collection time of a few minutes and in 10 mM PBS. In the control experiment, the ΔI_P values generated by CNEs at the same concentration of G and 8-OHdG are lower than the corresponding values acquired from the fGNEs, indicating the higher sensitivity of the fGNE after gold deposition of the CNE (Fig. S8A and C†).

It has been demonstrated that the electrochemical oxidation of G can be controlled by the electrode potential sweep rate.[23] As shown in Fig. 2E, when the sweep rate is high (20 V s^{-1}), G undergoes the two-electron oxidation process, forming 8-OXOG and its minor tautomer 8-OHGua. In contrast, when the electrode potential sweep rate is low (V = 0.05 V s^{-1}), G loses four electrons to form 8-OXOG (OX) (Fig. S9A†). As shown in Fig. 2F, after we sweep the electrode potential on the fGNE at 20 V s^{-1} for 50 cycles, a clear oxidation peak appears at +0.42 V in the DPV, which is down-shifted from +0.71 V. This oxidation peak becomes stable in the DPV at 50 mV s^{-1} and the peak position is consistent with the peak of 8-OXOG reported before.[46–49] Therefore, the down-shifted oxidation

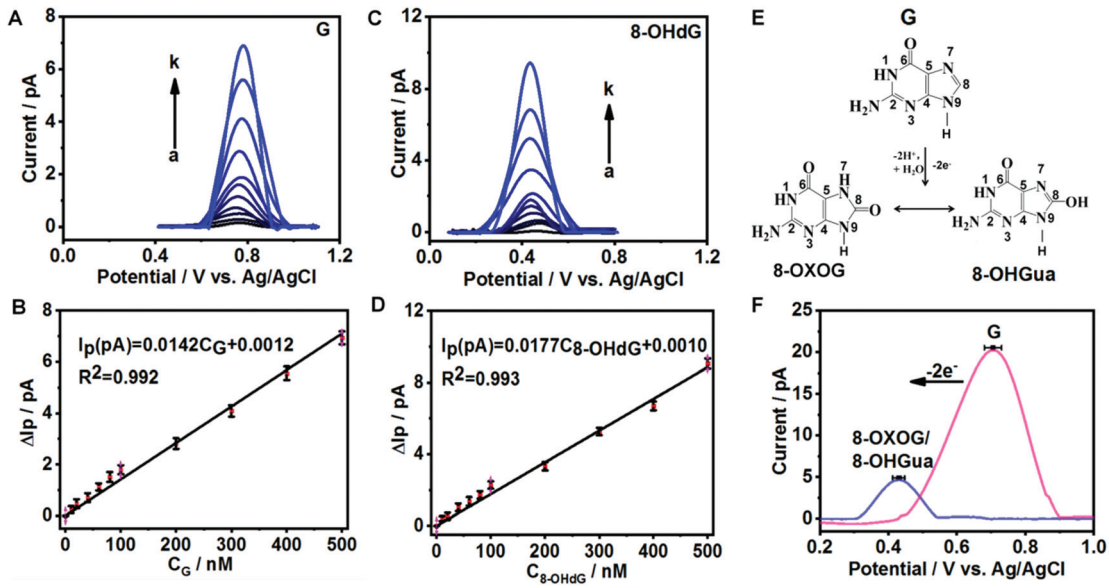

Fig. 2 Electrochemical detection of G and 8-OHdG with the fGNE. (A, C) DPVs of G and 8-OHdG at different concentrations (from a to k, 0, 10, 20, 40, 60, 80, 100, 200, 300, 400, and 500 nM, respectively) in 10 mM PBS. The scan rate is 50 mV s^{-1}. (B, D) The peak current (ΔI_P) at different concentrations of G and 8-OHdG. The error bars represent standard deviations. (E) Diagram of the two-electron electrochemical oxidation of G on the surface of fGNEs. (F) The oxidative peaks before (pink) and after (purple) the completion of the two-electron transfer process of G. The error bar represents the standard deviation.

peak confirms the two-electron oxidation transformation from G to 8-OXOG/8-OHGua on the fGNE apex surface. In contrast, after continuously sweeping the G-modified fGNE for 50 cycles with a low sweep rate of 50 mV s^{-1}, the oxidation peak is up-shifted from +0.71 V to +0.78 V in the DPV (Fig. S9B†), suggesting that the four-electron oxidation occurs and the oxidation product is not 8-OXOG or 8-OHGua. We also noticed that the 8-OXOG/8-OHGua oxidation peak is very close to the oxidation peak of 8-OHdG in Fig. 2C. Therefore, we cannot further differentiate the base or nucleotide forms of oxidative G from the oxidation peak in the DPV measurements.

SERS detection of G and its oxidative derivatives

G or its derivatives attached to fGNEs were also measured by SERS. The tip of the fGNE was first immersed in an aqueous solution (DI water) with 10 nM G or 8-OHdG for a few minutes. AgNPs were then introduced to the fGNE apex to enhance the intensity of SERS spectra, as described in the experimental methods and shown in Fig. 1C.

The typical Raman results are shown in Fig. 3. The G peaks can be identified in the normal Raman spectrum of G powder, as shown in Fig. 3A. The peaks in the SERS spectrum of G are generally broader and slightly shifted. The most noticeable peaks in the SERS spectrum of G are at 643, 934, 1342, 1381 and 1529 cm^{-1}. The assignments of these peaks are shown in Table S1.†

The Raman spectrum of the 8-OHdG powder and the SERS spectrum of adsorbed 8-OHdG on the fGNE tip are shown in Fig. 3B. For the 8-OHdG powder, four characteristic peaks appeared at 473, 637, 1443 and 1602 cm^{-1}. Compared with the normal Raman spectra, more spectral fluctuations are observed in the SERS spectra, as shown in three SERS spectra of 8-OHdG collected from different fGNEs under the same conditions in Fig. S10.† New peaks are observed near 1305 and 1381 cm^{-1}. The peaks at 660, 1381 and 1580 cm^{-1} almost always appeared. In particular, the 1580 cm^{-1} peak is down-shifted from 1602 cm^{-1} in the normal Raman spectrum. These changes are likely induced by the metal–molecule interactions on the gold surface.

The SERS spectrum of 8-OXOG/8-OHGua is also shown in Fig. 3B, which is collected after the two-electron oxidation of G on the fGNE. The major peaks are similar to the ones of adsorbed 8-OHdG on the fGNE. The 1381 cm^{-1} peak shifted slightly to around 1390 cm^{-1}. Other than that, it is generally difficult to differentiate 8-OXOG/8-OHGua from 8-OHdG in the SERS spectra. Between the SERS spectra of G and its two-electron oxidation derivatives 8-OXOG/8-OHGua or 8-OHdG, the characteristic peak of G at 643 cm^{-1} is much stronger than the corresponding peak of 8-OHdG/8-OHGua/8-OXOG near 660 cm^{-1}. Therefore, this peak can be used to differentiate G from its two-electron oxidative derivatives. We also measured the SERS spectrum of 8-OXOG (OX) after the four-electron oxidation on the fGNE (see Fig. S9C†). The SERS spectra of 8-OXOG (OX) are noticeably different from those of G or 8-OXOG/8-OHGua/8-OHdG. The SERS spectra of the other three DNA bases, A, T and C, were also measured on the fGNE surface. The characteristic peaks of G and its two-electron oxidation derivatives are quite different from those of the other three DNA bases and thus can be identified using the SERS spectra (Fig. S11†).[50]

To mimic the cell detection experiment (see the next paragraph), the fGNE was also immersed in MEM with various 8-OHdG concentrations, and a −70 mV bias voltage was applied for 40 min before the SERS measurements. Fig. 3B shows the typical SERS spectrum (orange color) for 0.1 nM 8-OHdG. With the applied bias and 40 min collection time, the intensity of the SERS peaks is obviously higher. Compared with the SERS spectrum of 8-OHdG adsorbed in DI water, the peak near 473 cm^{-1} appeared more often. The 1381 cm^{-1} peak often splitted into two peaks at 1371 and 1394 cm^{-1}. The peak at 1580 cm^{-1} is further downshifted to 1560 cm^{-1}. These spectral changes are likely due to the co-adsorbed interfering molecules, which are from the MEM medium, on the fGNE. The 1394 cm^{-1} peak is always the highest peak in the spectra. Therefore, we used the 1394 peak as the signature peak for 8-OHdG detection in MEM. As shown in Fig. 3C, the intensity of the 1394 peak (I_{1394}) increased linearly with an increase of the 8-OHdG concentration in MEM. The corresponding

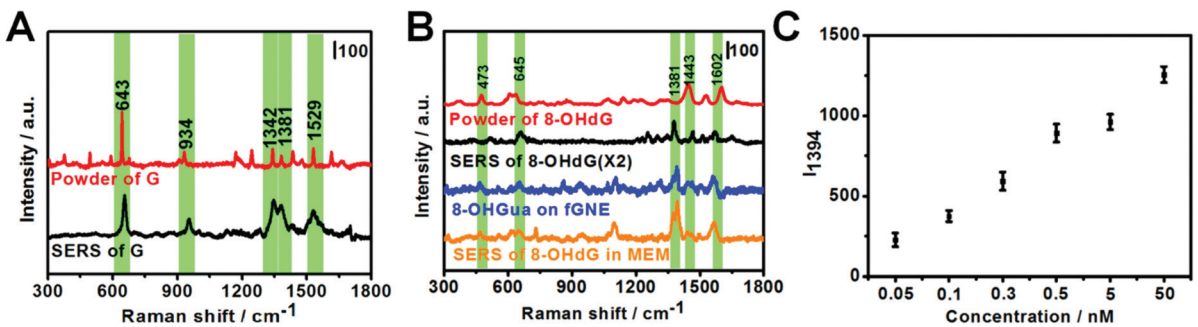

Fig. 3 Raman spectra of G derivatives. (A) Raman spectrum of the G powder and SERS spectrum of G. (B) Raman spectrum of the 8-OHdG powder (red), SERS spectrum of the fGNE after immersing in DI water with 10 nM 8-OHdG (black), SERS spectrum of 8-OHGua oxidized from G on the fGNE (blue), and SERS spectrum of the fGNE after immersing in MEM with 0.1 nM 8-OHdG (orange). The spectra are offsetted for clarity. (C) The SERS peak intensity of I_{1394} for fGNEs that were immersed in MEM solutions with different concentrations of 8-OHdG. The error bar represents the standard deviations.

Table 1 Characteristic Raman peaks (cm^{-1}) of 8-OHdG[45,46]

Calculated	Powder	SERS (adsorbed in DI water)	SERS (adsorbed in MEM)	Assignments
453	473	431	473	Wag N7–H, N9–H
646	637	660	650	Whole-molecule ring breathing
1300		1305	1295	Rock N1–H, str C5–C6
1372		1382	1371/1394	Rock N1–H, bend N1–C2–N3, N9–C4, def R5, R6
1455	1443	1468		Str N1–C2, sqz C4–C5, rock NH2
1568	1602	1580	1560	Str N7–C8O–N9, C6O–C5–C6

R5, five-membered ring; R6, six-membered ring; bend, bending; def, deformation; rock, rocking; sciss, scissoring; sqz, squeezing; str, stretching; wag, wagging.

spectra of these data points are shown in Fig. S12.† Considering a S/N ratio of 3, the LOD is about 0.1 nM for the SERS detection of 8-OHdG by the fGNE using −70 mV bias and 40 min collection time in MEM. Regarding the LOD, the SERS method is better than the DPV method.

In Table 1, we have presented the characteristic Raman peaks of 8-OHdG generated from the DFT calculation and the 8-OHdG powder and the SERS peaks from 8-OHdG-modified fGNEs with their adsorption in DI water or MEM.

Probing the oxidative DNA damage products in living cells by the fGNE

After demonstrating 8-OXOG/8-OHGua and 8-OHdG detection by the fGNE using electrochemical and SERS techniques in a controlled environment, we applied the fGNE for detecting oxidation damage products of DNA in live cells. The kidney epithelial Vero cells were exposed to 20 μM K_2CrO_4 or H_2O_2 for 2 h. It has been found that the cells can complete the DNA damage repair within two hours and maintain the normal physiological state of the cells.[51] The cell viability after the DNA damage treatment was also tested using the trypan blue exclusion test, and almost no dead cell was found at the used dosage (Fig. S13†). Then, the treated cells were placed in a fresh serum-free medium. Controlled by a micromanipulator, the fGNE slowly approached toward the cell until a small movement deformation of the cell membrane was observed in the optical image under a ×20 objective lens, suggesting that the apex already touched the cell surface (Fig. S14†). Then the tip apex was withdrawn about 2 μm, at which distance the cellular deformation disappeared. We defined this point as d_0, and other fGNE–cell distances were determined by withdrawing a defined distance from d_0 (see Fig. 4A). Facilitated by an applied bias of −70 mV to the fGNE, negatively charged DNA oxidation damage products were collected and attached to the surface of the fGNE. During the entire collection process of 40 min, the cells appear in a good condition in the culture medium MEM, without changes in their shape, volume, morphology, and substrate attachment.

After collecting the damage products, the fGNE was placed in 10 mM PBS for DPV measurements. A clear peak around a potential of 0.5 V was observed (Fig. 4B), which is slightly higher than the oxidative peak of 8-OHdG or oxidized G base products 8-OXOG/8-OHGua near 0.43 V in the previous characterization (Fig. 2C). Considering that the DNA damage products were collected in the cell culture medium, we speculated that other substances adsorbed on the electrode surface hinder the electron transfer of oxidized G bases and nucleotides and increase their oxidation potential. The electrochemical current is also dependent on the collecting distance between the fGNE tip and cell membrane. The DPV peak current was higher at a distance d_0 than that at d_0 + 30 μm. This is attributed to the adsorption of more competitive substances (such as proteins) to the electrode surface. These competitive substances likely suppressed or blocked the electron transfer of the newly attached oxidized G bases and nucleotides, which is called electrode fouling. Therefore, chemical modification to the gold surface will be needed to improve the sensitivity of the DPV method in live cell measurements.

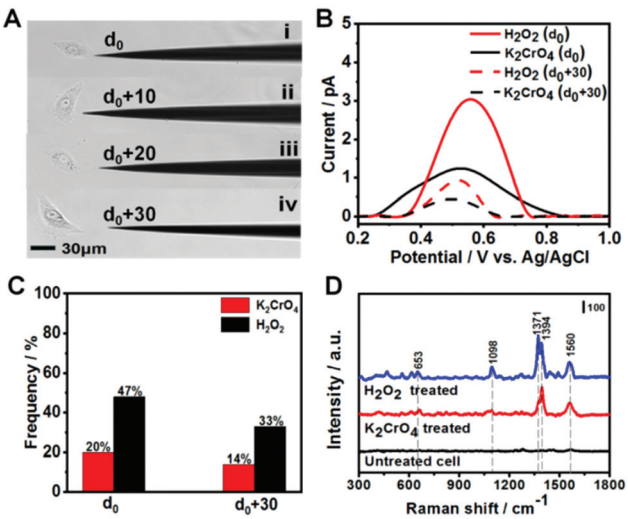

Fig. 4 Detecting the DNA damage products in living cells. (A) Optical image of the different distances between the fGNE and cell membrane controlled by a micromanipulator. (B) The DPV peaks of damage products collected on the fGNE with different distances (d_0, solid line; d_0 + 30 μm, dotted line) after treating cells with a final concentration of 20 μM K_2CrO_4 (black) and H_2O_2 (red). (C) The probability of observing DPV peaks of 8-OHdG on fGNEs after collecting the damage products at distances d_0 and d_0 + 30 μm (N = 15). (D) SERS of the DNA damage products on the fGNEs measured at distance d_0. The collection time is always 40 min.

Although the DPV cannot accurately measure the released amount of DNA damage products, the DPV results still suggest that both K_2CrO_4 and H_2O_2 treatments can cause damage to the DNA of Vero cells and lead to the release of oxidized G bases and nucleotides. As we have shown in the previous section, the fGNE also effectively collects them. However, due to electrode fouling, only a fraction of fGNEs can observe the DPV peak near 0.5 V. This percentage also depends on the type of DNA damage agent and the distance between the fGNE tip and the cell membrane. As shown in Fig. 4C, when the fGNEs are at d_0, the probability to detect the DPV peak near 0.5 V is 20% for K_2CrO_4 and 47% for H_2O_2, respectively. When the fGNEs are at d_0 + 30 μm, the appearance probability is 14% for K_2CrO_4 and 33% for H_2O_2, respectively. Between K_2CrO_4 and H_2O_2 treatments, the latter always induces a higher DPV peak at a potential of 0.5 V. This is reasonable considering H_2O_2 is a stronger oxidant; it causes greater oxidative damage to DNA, leading to a higher level of released oxidized G bases and nucleotides after self-repairing.

To further analyze the DNA damage products, SERS measurements were conducted to detect the attached DNA damage products on the apex surface of fGNEs. Fig. 4D shows the typical SERS spectra from fGNEs after collecting DNA damage products from Vero cells treated with 20 μM K_2CrO_4 or H_2O_2 for 2 h. No clear SERS peaks can be identified for untreated Vero cells. In contrast, clear and almost identical peaks can be observed after K_2CrO_4 or H_2O_2 treatment. In both spectra, pronounced peaks appeared at 653, 1394, and 1560 cm^{-1}. These peaks are consistent with the SERS peaks of 8-OHdG collected in MEM. Therefore, the SERS measurement further confirmed the successful collection of 8-OHdG or 8-OXOG on the fGNE apex. The signature peak of G near 643 cm^{-1} cannot be clearly identified in the spectra. Therefore, the amount of free G or dG and GTP in the extracellular medium is very low compared with the oxidized G products, which were released by the cell after various DNA repair mechanisms. By using Fig. 3C with spiked 8-OHdG as the calibration curve, the amount of oxidized G products released from a single cell can be roughly estimated by comparing the intensity of I_{1394}. Although there are cell-to-cell fluctuations in I_{1394}, the concentration of the released oxidized G products near the cell surface is generally less than 0.1 nM after K_2CrO_4 treatment. It is also found that the SERS intensity of the peaks of the oxidized G products from H_2O_2-treated cells is always higher than that of K_2CrO_4-treated cells, suggesting that more oxidized G products were released after H_2O_2 treatment. This is consistent with the DPV measurement.

To optimize the collection of oxidized G products, we first varied the distance between the fGNE apex and cell surface. As shown in Fig. 5A, I_{1394} increases when the fGNE apex is moved away from the cell membrane surface. Interestingly, this is opposite to the DPV results. When the fGNE is away from the cell membrane surface, it has the chance to collect more oxidized G products released from nearby cells. However, more competitive substances are also likely attached to the fGNE. These interferences made a bigger impact on the electrochemical current but contribute much less to the SERS signal. This result also underscores the importance of combined electrochemical and SERS measurements. Subsequently, we varied the collection time while fixing the distance between the fGNE and cell membrane at d_0. As shown in Fig. 5B, I_{1394} increases with the increase of the collection time and reaches a maximum at 60 min. Interestingly, beyond 60 min, I_{1394} gradually decreases. One plausible explanation is that the cells actively repair DNA damage induced by the treatment in the first 60 min. After 60 min, the level of released oxidized G products gradually decreases. However, the decrease of I_{1394} may also be due to the saturation of the electrode. To test this possibility, we performed control experiments in the cell culture medium MEM (but without cells) with various concentrations of 8-OHdG (Fig. S15†). We found that I_{1394} continues to increase beyond 60 min as the collection time increases. Therefore, the decrease of the I_{1394} peak after 60 min in cellular measurements should be related to the recovery of cells after self-repair.

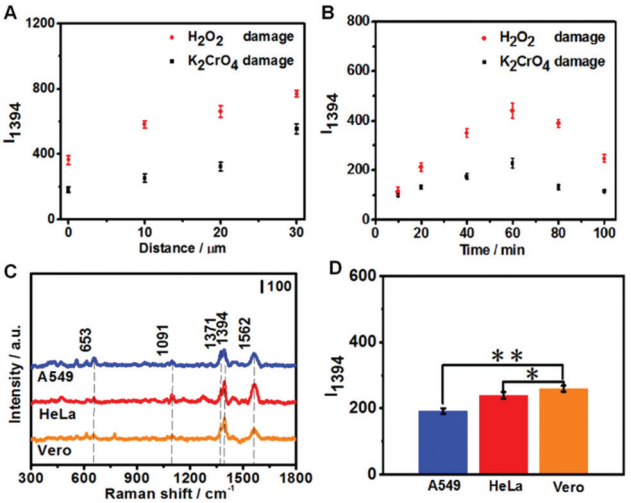

Fig. 5 The SERS peak intensity I_{1394} of fGNEs under different conditions. (A) The I_{1394} value that collects the damage products for 40 min at different distances from the cell after K_2CrO_4 or H_2O_2 treatment. (B) The I_{1394} value that collects the damage products of cells for different times with distance d_0 after K_2CrO_4 or H_2O_2 treatments. (C) The SERS spectra of fGNEs that collect the damage products resulting from three different cell lines at distance d_0 after treatment with K_2CrO_4. (D) The intensity histograms of I_{1394} for fGNEs that collect the damage products resulting from three different cell lines at distance d_0 after treatment with K_2CrO_4. Two-tailed Student's *t*-test: $^*P < 0.05$, $^{**}P < 0.01$.

We further performed the measurements on two cancer cell lines (A549 and HeLa) under the same conditions. Three cell lines were both treated with 20 μM K_2CrO_4 for 2 h; then the fGNE was used to collect DNA damage products from individual cells at d_0 for 40 min. It can be seen from Fig. 5C that similar SERS spectra were acquired from all three cell lines. However, the I_{1394} value of Vero cells is slightly higher than those of the other two cell lines (Fig. 5D), which is attributed to the higher resistance of cancer cells to environmental damage.

Conclusions

In summary, we have successfully prepared a fGNE for collecting and detecting DNA damage products released by individual live cells. To evaluate its capability to detect DNA damage products, we first tested the performance of the fGNE by using the most common DNA damage biomarkers 8-OHdG and 8-OXOG. The base form of G oxidative products can be acquired by electrochemical oxidation of the tethered G on the electrode. When the electrode potential scanning speed is high, G is mainly oxidized to 8-OXOG. fGNEs show high sensitivity and selectivity toward oxidative G products in the integrated electrochemistry and SERS measurements. By analyzing the oxidation potential of the DPV peak and the molecular fingerprints in the SERS spectra, we can confirm that the attached molecules are mainly oxidative G products instead of G or 8-OXOG (OX) or other non-G interferences. However, we cannot further determine the detailed structure of oxidized G products, including whether they are in base or nucleotide forms and with which tautomer structures.

In the cellular measurements, the cells were treated with K_2CrO_4 or H_2O_2. By controlling the distance between the fGNE tip and the cell membrane, the collection time and the applied bias, we can optimize the collecting conditions and enhance the detection of released oxidative DNA damage products. Based on the DPV and SERS results, we can determine that mainly G oxidative products were released from the cell after both treatments. We found that at the same treatment dosage, more oxidative G products were generated by H_2O_2 treatment than K_2CrO_4 treatment. Similar detection results have been acquired in three different cell lines, HeLa, A549, and Vero. However, the cancer cells A549 and HeLa normally generated less DNA damage products than the normal cells Vero. The SERS measurement can overcome electrode fouling and show much better LOD (~0.1 nM) for oxidative G and dG products than the DPV measurement. The detection limit by SERS is comparable to or better than a lot of methods for 8-OHdG detection in biofluids.[25,52,53] Here, the electrode is not functionalized, and we relied on the strong Au–N interaction between gold and oxidative G. In recently reported works, aptamer-involved EC and spectroscopy methods can further improve the detection limit of 8-OHdG to the picomolar concentration.[52,53] Similar chemical modification strategies, as well as other nanostructured materials,[25] should also be adopted by the fGNE method to further improve its specificity and sensitivity and enable real-time detection by the electrochemical method. We also envision that the fGNE-based integrated analytical approaches can be applied for both intracellular detection and extracellular detection of other important cellular biomarkers at the single-cell level.

Conflicts of interest

There are no conflicts to declare.

Acknowledgements

This work was supported by the National Natural Science Foundation of China (21673023 and 21773017). We acknowledge Jianghao Zhou for help with DFT calculations.

Notes and references

1 M. S. Cooke, M. D. Evans, M. Dizdaroglu and J. Lunec, *FASEB J.*, 2003, **17**, 1195–1214.
2 S. P. Jackson and J. Bartek, *Nature*, 2009, **461**, 1071–1078.
3 J. Cadet, J. R. Wagner, V. Shafirovich and N. E. Geacintov, *Int. J. Radiat. Biol.*, 2014, **90**, 423–432.
4 S. Steenken and S. V. Jovanovic, *J. Am. Chem. Soc.*, 1997, **119**, 617–618.
5 E. C. Friedberg, *Nature*, 2003, **421**, 436–440.
6 M. S. Cooke, M. D. Evans, K. E. Herbert and J. Lunec, *Free Radical Res.*, 2000, **32**, 381–397.
7 C.-Y. Ock, E.-H. Kim, D. J. Choi, H. J. Lee, K.-B. Hahm and M. H. Chung, *World J. Gastroenterol.*, 2012, **18**, 302–308.
8 S. F. Lee and S. Pervaiz, in *Methods in Cell Biology*, ed. Z. Darzynkiewicz, E. Holden, A. Orfao, W. Telford and D. Wlodkowic, Academic Press, 2011, vol. 103, pp. 99–113.
9 B. Halliwell and M. Whiteman, *Br. J. Pharmacol.*, 2004, **142**, 231–255.
10 H. J. Helbock, K. B. Beckman and B. N. Ames, in *Methods in Enzymology*, Academic Press, 1999, vol. 300, pp. 156–166.
11 L. L. Wu, C.-C. Chiou, P.-Y. Chang and J. T. Wu, *Clin. Chim. Acta*, 2004, **339**, 1–9.
12 M. A. Lovell and W. R. Markesbery, *Nucleic Acids Res.*, 2007, **35**, 7497–7504.
13 I. Dalle-Donne, R. Rossi, R. Colombo, D. Giustarini and A. Milzani, *Clin. Chem.*, 2006, **52**, 601–623.
14 M. Dizdaroglu, P. Jaruga and H. Rodriguez, *Nucleic Acids Res.*, 2001, **29**, e12–e12.
15 S. Koide, Y. Kinoshita, N. Ito, J. Kimura, K. Yokoyama and I. Karube, *J. Chromatogr. B: Anal. Technol. Biomed. Life Sci.*, 2010, **878**, 2163–2167.
16 B. Halliwell and M. Dizdaroglu, *Free Radical Res. Commun.*, 1992, **16**, 75–87.
17 S. Mahajan, T.-C. Lee, F. Biedermann, J. T. Hugall, J. J. Baumberg and O. A. Scherman, *Phys. Chem. Chem. Phys.*, 2010, **12**, 10429.
18 B. Yin, R. M. Whyatt, F. P. Perera, M. C. Randall, T. B. Cooper and R. M. Santella, *Free Radicals Biol. Med.*, 1995, **18**, 1023–1032.
19 K. Shimoi, H. Kasai, N. Yokota, S. Toyokuni and N. Kinae, *Cancer Epidemiol., Biomarkers Prev.*, 2002, **11**, 767–770.
20 R. P. Soultanakis, R. J. Melamede, I. A. Bespalov, S. S. Wallace, K. B. Beckman, B. N. Ames, D. J. Taatjes and Y. M. W. Janssen-Heininger, *Free Radicals Biol. Med.*, 2000, **28**, 987–998.
21 A. R. Collins, J. Cadet, L. Mőller, H. E. Poulsen and J. Viña, *Arch. Biochem. Biophys.*, 2004, **423**, 57–65.

22 K. S. Korkmaz, B. Debelec Butuner and D. Roggenbuck, *J. Lab. Precis. Med.*, 2018, **3**, 95–95.
23 E. E. Ferapontova, *Electrochim. Acta*, 2004, **49**, 1751–1759.
24 J. Langmaier, Z. Samec and E. Samcová, *Electroanalysis*, 2003, **15**, 1555–1560.
25 A. M. Chiorcea-Paquim and A. M. Oliveira-Brett, *Mikrochim. Acta*, 2021, **188**, 58.
26 S. Prabhulkar and C.-Z. Li, *Biosens. Bioelectron.*, 2010, **26**, 1743–1749.
27 P. Actis, S. Tokar, J. Clausmeyer, B. Babakinejad, S. Mikhaleva, R. Cornut, Y. Takahashi, A. López Córdoba, P. Novak, A. I. Shevchuck, J. A. Dougan, S. G. Kazarian, P. V. Gorelkin, A. S. Erofeev, I. V. Yaminsky, P. R. Unwin, W. Schuhmann, D. Klenerman, D. A. Rusakov, E. V. Sviderskaya and Y. E. Korchev, *ACS Nano*, 2014, **8**, 875–884.
28 J. Zhang, J. Zhou, R. Pan, D. Jiang, J. D. Burgess and H.-Y. Chen, *ACS Sens.*, 2018, **3**, 242–250.
29 S.-M. Lu and Y.-T. Long, *TrAC, Trends Anal. Chem.*, 2019, **117**, 39–46.
30 J. Guo, A. Sesena Rubfiaro, Y. Lai, J. Moscoso, F. Chen, Y. Liu, X. Wang and J. He, *Analyst*, 2020, **145**, 4852–4859.
31 S. Hanif, H.-L. Liu, S. A. Ahmed, J.-M. Yang, Y. Zhou, J. Pang, L.-N. Ji, X.-H. Xia and K. Wang, *Anal. Chem.*, 2017, **89**, 9911–9917.
32 E. A. Vitol, Z. Orynbayeva, M. J. Bouchard, J. Azizkhan-Clifford, G. Friedman and Y. Gogotsi, *ACS Nano*, 2009, **3**, 3529–3536.
33 P. H. Acioli and S. Srinivas, *J. Mol. Model.*, 2014, **20**, 2391.
34 X. Zhang, C. Q. Sun and H. Hirao, *Phys. Chem. Chem. Phys.*, 2013, **15**, 19284–19292.
35 K. D. Sugden, C. K. Campo and B. D. Martin, *Chem. Res. Toxicol.*, 2001, **14**, 1315–1322.
36 H. W. Kuo, *Occup. Environ. Med.*, 2003, **60**, 590–594.
37 Y. Fujii, K. Tomita, H. Sano, A. Yamasaki, Y. Hitsuda, I. M. Adcock and E. Shimizu, *Cancer Cell Int.*, 2002, **2**, 16.
38 H. Kasai, P. F. Crain, Y. Kuchino, S. Nishimura, A. Ootsuyama and H. Tanooka, *Carcinogenesis*, 1986, **7**, 1849–1851.
39 S. Agnihotri, S. Mukherji and S. Mukherji, *RSC Adv.*, 2014, **4**, 3974–3983.
40 N. Panday, G. Qian, X. Wang, S. Chang, P. Pandey and J. He, *ACS Nano*, 2016, **10**, 11237–11248.
41 D. Yang, G. Liu, H. Li, A. Liu and J. He, *Analyst*, 2020, **145**(3), 1047–1055.
42 F. Lussier, T. Brule, M. J. Bourque, C. Ducrot, L. É. Trudeau and J. F. Masson, *Faraday Discuss.*, 2017, **205**, 387–407.
43 H. Schmidbaur, H. G. Raubenheimer and L. Dobrzańska, *Chem. Soc. Rev.*, 2014, **43**, 345–380.
44 J. Zhang, D. Han, S. Wang, X. Zhang, R. Yang, Y. Ji and X. Yu, *Electrochem. Commun.*, 2019, **99**, 75–80.
45 I. Pandey and J. D. Tiwari, *Sens. Actuators, B*, 2019, **285**, 470–478.
46 G. V. Martins, A. P. M. Tavares, E. Fortunato and M. G. F. Sales, *Sci. Rep.*, 2017, **7**, 14558.
47 Z. Guo, X. Liu, Y. Liu, G. Wu and X. Lu, *Biosens. Bioelectron.*, 2016, **86**, 671–676.
48 F. D'Amico, F. Cammisuli, R. Addobbati, C. Rizzardi, A. Gessini, C. Masciovecchio, B. Rossi and L. Pascolo, *Analyst*, 2015, **140**, 1477–1485.
49 N. Jayanth, S. Ramachandran and M. Puranik, *J. Phys. Chem. A*, 2009, **113**, 1459.
50 J.-M. Yang, L. Jin, Z.-Q. Pan, Y. Zhou, H.-L. Liu, L.-N. Ji, X.-H. Xia and K. Wang, *Anal. Chem.*, 2019, **91**, 6275–6280.
51 A. S. Rubfiaro, P. S. Tsegay, Y. Lai, E. Cabello, M. Shaver, J. Hutcheson, Y. Liu and J. He, *ACS Appl. Bio Mater.*, 2021, **4**(2), 1632–1639.
52 Y. Liu, M. Wei, L. Zhang, Y. Zhang, W. Wei, L. Yin, Y. Pu and S. Liu, *Anal. Chem.*, 2016, **88**, 6509–6514.
53 J. Fan, Y. Liu, E. Xu, Y. Zhang, W. Wei, L. Yin, Y. Pu and S. Liu, *Anal. Chim. Acta*, 2016, **946**, 48–55.